Familial Alzheimer disease–linked mutations specifically disrupt Ca^{2+} leak function of presenilin 1

Omar Nelson,[1] Huiping Tu,[1] Tianhua Lei,[1] Mostafa Bentahir,[2] Bart de Strooper,[2] and Ilya Bezprozvanny[1]

[1]Department of Physiology, University of Texas Southwestern Medical Center at Dallas, Dallas, Texas, USA. [2]Center for Human Genetics, Katholieke Universiteit Leuven, and Department for Molecular and Developmental Genetics, Flanders Institute for Biotechnology, Leuven, Belgium.

Mutations in presenilins are responsible for approximately 40% of all early-onset familial Alzheimer disease (FAD) cases in which a genetic cause has been identified. In addition, a number of mutations in presenilin-1 (PS1) have been suggested to be associated with the occurrence of frontal temporal dementia (FTD). Presenilins are highly conserved transmembrane proteins that support cleavage of the amyloid precursor protein by γ-secretase. Recently, we discovered that presenilins also function as passive ER Ca^{2+} leak channels. Here we used planar lipid bilayer reconstitution assays and Ca^{2+} imaging experiments with presenilin-null mouse embryonic fibroblasts to analyze ER Ca^{2+} leak function of 6 FAD-linked PS1 mutants and 3 known FTD-associated PS1 mutants. We discovered that L166P, A246E, E273A, G384A, and P436Q FAD mutations in PS1 abolished ER Ca^{2+} leak function of PS1. In contrast, A79V FAD mutation or FTD-associated mutations (L113P, G183V, and Rins352) did not appear to affect ER Ca^{2+} leak function of PS1 in our experiments. We validated our findings in Ca^{2+} imaging experiments with primary fibroblasts obtained from an FAD patient possessing mutant PS1-A246E. Our results indicate that many FAD mutations in presenilins are loss-of-function mutations affecting ER Ca^{2+} leak activity. In contrast, none of the FTD-associated mutations affected ER Ca^{2+} leak function of PS1, indicating that the observed effects are disease specific. Our observations are consistent with the potential role of disturbed Ca^{2+} homeostasis in Alzheimer disease pathogenesis.

Introduction

Alzheimer disease (AD) is the most common form of age-related dementia in human beings over the age of 60 years. AD affects about 2% of populations in industrialized countries. The understanding of the molecular processes that lead to the pathogenesis of AD is immensely important in combatting this neurological disease. Most cases of AD are idiopathic and are characterized by late onset (in individuals over 60 years of age). A small fraction of AD cases (familial AD [FAD]) are characterized by an earlier onset and genetic inheritance. Mutations in presenilin-1 (PS1) and PS2 account for about 40% of all known FAD cases in which a genetic cause has been identified (1). Three missense mutations in PS1 have been suggested to be associated with frontal temporal dementia (FTD) (2), a neurological disorder that affects the frontal and temporal lobes of the brain. Presenilins are 50-kD proteins that contain 9 transmembrane domains (3, 4) and reside in the ER membrane (5). The complex of presenilins, that includes aph-1 and pen-2 subunits, is transported to the cell surface and endosomal structures, where it functions as γ-secretase. The γ-secretase cleaves the amyloid precursor protein (APP) and releases the amyloid β-peptide, the principal constituent of the amyloid plaques in the brains of AD patients. Consistent with the role of presenilins as catalytic subunits of γ-secretase (6, 7), FAD mutations in presenilins affect APP processing.

In addition to changes in APP processing, many FAD mutations in presenilins result in deranged Ca^{2+} signaling (reviewed in ref. 8). Although the connection between FAD mutations in presenilins and abnormal Ca^{2+} signaling has been known for over a decade (9), the mechanistic explanation for this finding has been controversial (8). Recently, we discovered that presenilins function as passive ER Ca^{2+} leak channels (10). We further found that PS1-M146V, PS1-ΔE9, and PS2-N141I FAD mutations in presenilins affected their ER Ca^{2+} leak function (10). In the present study, we used planar lipid bilayer (BLM) reconstitution assays and Ca^{2+} imaging experiments with presenilin-null mouse embryonic fibroblasts (MEFs) to analyze ER Ca^{2+} leak function of 6 additional PS1 FAD mutants. Our results indicate that many FAD mutations in PS1 disrupt ER Ca^{2+} leak function. These observations provide further support for the contribution of disturbed Ca^{2+} homeostasis to AD pathogenesis (8, 11–13). In addition, we discovered that none of the 3 suggested FTD-associated PS1 mutations affected ER Ca^{2+} leak function of PS1. These results indicate that the effects of FAD mutations on ER Ca^{2+} leak function of presenilins are disease specific.

Results

Ca^{2+} channel function of PS1 FAD mutants in BLMs. Predicted structure of presenilins includes 9 transmembrane domains (3, 4) (Figure 1A), consistent with potential ion channel or transporter function. In a previous study, we discovered that presenilin holoproteins function as passive ER Ca^{2+} leak channels (10). We further discovered that PS1-M146V, PS1-ΔE9, and PS2-N141I FAD mutations (Figure 1A) affected their ER Ca^{2+} leak function, whereas PS1-D257A γ-secretase catalytic mutation was without effect (10). In the present study, we set out to test ER Ca^{2+} leak function of 6 additional PS1

Nonstandard abbreviations used: AD, Alzheimer disease; BK, bradykinin; BLM, planar lipid bilayer; $[Ca^{2+}]_{ER}$, ER Ca^{2+} concentration; DKO, double knockout; EGFP, enhanced GFP; FAD, familial AD; FTD, frontal temporal dementia; hF, human fibroblast; IO, ionomycin; MEF, mouse embryonic fibroblast; PS1, presenilin-1.

Conflict of interest: I. Bezprozvanny received consulting payments from EnVivo Inc., which also funded a project in his lab, in 2006.

Citation for this article: *J. Clin. Invest.* **117**:1230–1239 (2007). doi:10.1172/JCI30447.

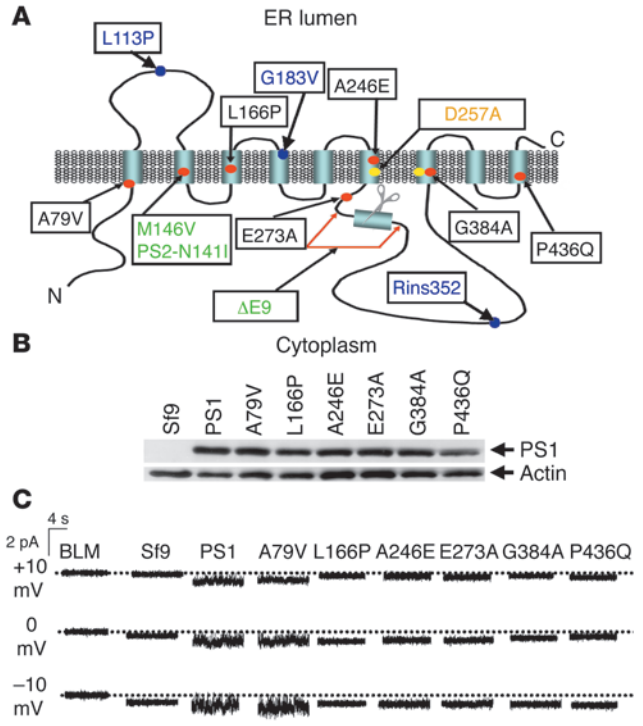

Figure 1
Recombinant presenilins form Ca^{2+} channels in BLMs. (**A**) Molecular model of presenilins (3, 4). The 9 transmembrane domains (TM1–TM9) of presenilins, the γ-secretase catalytic aspartate residues (yellow dots), and the site of the endoproteolytic cleavage (scissors) are shown. The positions of PS1 FAD mutants A79V, L166P, A246E, E273A, G384A, and P436Q examined in our study are shown (red dots, black letters). Also shown are positions of M146V, ΔE9 FAD mutations in PS1, and N141I FAD mutations in PS2 analyzed in ref. 10 (red dots, green letters). Also shown is D257A "γ-secretase" mutation in PS1, which was analyzed in ref. 10 (yellow dot, orange letters) and FTD-associated PS1 mutations L113P, G183V, and Rins352 examined in our study (blue dots, blue letters). (**B**) Expression of PS1 and PS1 mutants in Sf9 cells. The ER microsomes from noninfected Sf9 cells and from Sf9 cells infected with WT and FAD mutant PS1-encoding baculoviruses were analyzed by Western blotting with anti-PS1 monoclonal antibodies. The position of PS1 holoprotein is indicated by an arrow. Actin was used as the loading control. (**C**) The Ba^{2+} currents recorded at +10 mV, 0 mV, and –10 mV holding potentials are shown for the empty BLM and for BLM fused with ER microsomal preparations from Sf9 cells infected with the WT and FAD mutant PS1-encoding baculoviruses. Similar results were obtained in at least 5 independent BLM experiments with each PS1 mutant.

FAD mutants — A79V, L166P, A246E, E273A, G384A, and P436Q (Figure 1A). The FAD mutations from different regions of the PS1 sequence were chosen for analysis (Figure 1A) to maximize coverage of our experiments. Baculoviruses encoding these 6 selected FAD PS1 mutants were generated, and recombinant WT PS1 and PS1 FAD mutants were expressed in Sf9 cells. Western blotting analysis confirmed that WT PS1 and all 6 FAD PS1 mutants were expressed at similar levels in baculovirus-infected Sf9 cells (Figure 1B). To study the ion channel function of recombinant PS1 and the PS1 FAD mutants, we performed BLM reconstitution experiments with ER microsomes from baculovirus-infected Sf9 cells. These experiments were performed as described in our previous study of the ion channel function of PS1 (10). Ba^{2+} ions (50 mM on *trans* side) were used in these experiments as a current carrier. We did not detect ion currents across the BLM prior to fusion of ER microsomes or following fusion of microsomes from noninfected Sf9 cells (Figure 1C). In contrast, when microsomes from PS1-infected Sf9 cells were fused to the BLM, Ba^{2+} currents were observed in our experiments (Figure 1C), consistent with our previous findings (10). A previous report indicated that the function of ER Ca^{2+} leak pathway may be modulated by millimolar levels of cytosolic ATP levels (14). We evaluated effects of ATP on PS1-mediated current activity in bilayers but did not observe significant effects (data not shown). Using noise analysis, we estimated that the unitary current size of PS1-supported channel was equal to 0.046 ± 0.004 pA (n = 3) in the absence of ATP and 0.041 ± 0.005 pA (n = 3) in the presence of 5 mM ATP on the cytosolic (*cis*) side of the bilayer, not significantly different from each other. In further bilayer experiments we determined that the PS1-A79V mutants supported Ba^{2+} currents across the BLM, similar to the WT PS1 (Figure 1C), but the other 5 mutants tested in our experiments were not active in the BLM (Figure 1C). By applying the previously described noise analysis algorithm (10), we estimated that at 0 mV transmembrane potential, the unitary Ba^{2+} current size was equal to 0.04 ± 0.01 pA (n = 5) for PS1-supported currents and 0.035 ± 0.003 pA (n = 4) for currents supported by PS1-A79V mutant (Table 1). Noise analysis further confirmed absence of detectable ion channel activity in experiments with L166P, A246E, E273A, G384A, and P436Q FAD mutants of PS1 (Table 1).

Rescue of Ca^{2+} signaling defects in presenilin double-knockout MEFs with FAD PS1 mutations. In the previous study (10), we described Ca^{2+} signaling defects in PS1/2 double-knockout (DKO) MEFs (15). Specifically, we found that the amplitude of bradykinin-induced (BK-induced) Ca^{2+} release (mediated by inositol 1,4,5-triphosphate ER Ca^{2+} channels) is twice as high in DKO MEFs as in WT MEFs (10). We further found that the application of the Ca^{2+} ionophore ionomycin (IO) resulted in more massive and longer-lasting Ca^{2+} signals in DKO cells than in MEFs (10), and that the intraluminal ER Ca^{2+} levels were significantly elevated in DKO cells compared with WT cells (10). As described in the previous study, all of these observations could be explained by defective ER Ca^{2+} leak pathway in DKO cells (10). To evaluate ER Ca^{2+} leak function of WT PS1 and selected PS1 FAD mutants, we performed a series of rescue experiments. In these experiments, DKO fibroblasts were transfected by enhanced GFP (EGFP) plasmid alone (EGFP control) or EGFP plasmid together with the PS1 expression constructs and analyzed by Fura-2 Ca^{2+} imaging 48 hours after transfection. The transfected cells in these experiments were identified by GFP fluorescence (Figure 2).

The resting Ca^{2+} levels in transfected DKO cells were estimated from Fura-2 340:380 ratio measurements. We found that the average basal Ca^{2+} level in DKO cells transfected with EGFP plasmid was equal to 186 ± 32 nM (n = 33) (Figure 3A). The average basal Ca^{2+} levels in DKO cells cotransfected with EGFP and L166P, A246E, E273A, G384A, and P436Q mutant PS1 expression plasmids were not significantly different from DKO cells transfected with EGFP plasmid alone (Figure 3A). In contrast, the mean basal Ca^{2+} level in DKO cells transfected with the EGFP+PS1 plasmid combination was equal to 263 ± 47 nM (n = 21), significantly higher than in DKO cells transfected with EGFP alone (P < 0.05) (Figure 3A).

Table 1
The effects of FAD mutations on ER Ca^{2+} leak function of presenilins

Cells and constructs	i (pA)	Transient			Stable			
		BK peak (nM)	IO area (μM•s)	ER Ca^{2+} (μM)	IO area (μM•s)	ER Ca^{2+} (μM)	Mean AAO	References
MEF	NA	234 ± 27	22 ± 8	97 ± 19	22 ± 8	97 ± 19	NA	
DKO	NA	752 ± 141	56 ± 16	183 ± 42	56 ± 16	183 ± 42	NA	
PS1	0.04 ± 0.01	271 ± 53	33 ± 9	108 ± 21	24 ± 5	93 ± 15	NA	
A79V	0.035 ± 0.003	253 ± 39	31 ± 14	114 ± 28	ND	ND	53–58	39
M146V	-	634 ± 125	49 ± 11	170 ± 36	ND	ND	32–39	39
L166P	-	714 ± 73	52 ± 14	227 ± 39	53 ± 9	178 ± 19	24	44
A246E	-	706 ± 92	51 ± 12	234 ± 47	54 ± 11	191 ± 23	53	39
ΔE9	0.09 ± 0.02	242 ± 76	20 ± 10	65 ± 20	23 ± 8	81 ± 30	36–55	39
E273A	-	674 ± 154	53 ± 9	210 ± 53	ND	186 ± 31	63	39
D257A	0.06 ± 0.01	219 ± 99	23 ± 5	70 ± 10	25 ± 11	ND	NA	
G384A	-	631 ± 133	50 ± 12	221 ± 42	57 ± 9	104 ± 36	31–37	39
P436Q	-	748 ± 124	48 ± 9	216 ± 59	ND	ND	20–42	39
PS2	0.03 ± 0.01	343 ± 58	ND	ND	34 ± 10	104 ± 36	NA	
N141I/L	-	617 ± 169	ND	ND	48 ± 19	211 ± 55	50–65	48
hF	NA	318 ± 71	84 ± 19	ND	19 ± 7	84 ± 19	NA	
hF-A246E	-	629 ± 114	169 ± 27	ND	37 ± 12	169 ± 27	53	39

The summary of results obtained in this study with A79V, L166P, A246E, E273A, G384A, P436Q, hF, and hF-A246E and in ref. 10 with MEF, DKO, PS1, M146V, ΔE9, D257A, PS2, and PS2-N141I is shown. The unitary size of Ba^{2+} currents estimated from noise analysis of BLM reconstitution experiments is shown for PS1, PS1-A79V, PS1-ΔE9, PS1-D257A, and PS2. No currents were observed in experiments with other FAD mutants tested. The average amplitude of BK-induced Ca^{2+} response, the average content of IO-sensitive Ca^{2+} pool and the mean $[Ca^{2+}]_{ER}$ are shown for WT MEFs, DKO cells, DKO cells transiently and stably transfected with presenilin rescue constructs, hFs, and PS1-A246E hFs. The FAD age of onset (AAO) for cases resulting from the same mutations is also shown. NA, not applicable; ND, not determined.

The mean basal Ca^{2+} level in DKO cells cotransfected with EGFP and A79V PS1 mutant plasmid was equal to 257 ± 34 nM (n = 40), also significantly higher (P < 0.05) than in DKO cells transfected with EGFP alone. To explain these results, we reasoned that the expression of WT PS1 and PS1-A79V mutant plasmids, but not the other 5 FAD PS1 mutants tested in our study increases passive Ca^{2+} leak from the ER and elevates basal cytosolic Ca^{2+} levels in transfected DKO cells.

When transfected DKO cells were challenged with 300 nM BK, large transient Ca^{2+} signals were observed in EGFP, EGFP+L166P–, EGFP+A246E–, EGFP+E273A–, EGFP+G384A–, and EGFP+P436Q–transfected cells (Figure 2). In contrast, significantly smaller Ca^{2+} signals were induced by BK in DKO cells transfected with EGFP+PS1 and EGFP+A79V combinations (Figure 2). On average, the difference between peak and basal Ca^{2+} levels ($\Delta[Ca^{2+}]$) in BK-stimulated cells was equal to 732 ± 103 nM (n = 33) for EGFP-transfected cells, 271 ± 53 nM (n = 21) for EGFP+PS1–transfected cells, and 253 ± 39 nM (n = 40) for EGFP+A79V–transfected cells (Figure 3A and Table 1). The peak responses in DKO cells transfected with the other FAD mutants were not significantly different from the peak Ca^{2+} responses in cell transfected with EGFP plasmid alone (Figure 3A and Table 1). Thus, transfection of DKO cells with WT PS1 and A79V expression constructs reduced the amplitude of BK-induced Ca^{2+} responses to levels observed in experiments with WT MEFs (Figure 3A and Table 1), whereas expression of L166P, A246E, E273A, G384A and P436Q FAD mutants had no significant effect on the amplitude of BK-induced responses (Figure 3A and Table 1).

In the next series of experiments we evaluated the size of IO-sensitive Ca^{2+} pool in PS1-transfected DKO cells. IO is an ionophore that induces formation of Ca^{2+}-permeable pores in cellular membranes, leading to complete emptying of ER Ca^{2+} stores independently from the inositol 1,4,5-triphosphate receptor activation. In agreement with the previous findings (10), we found that addition of 5 μM IO induced large and long-lasting elevation of cytosolic Ca^{2+} levels in EGFP-transfected DKO cells, but smaller in amplitude and shorter in duration in EGFP+PS1–transfected cells (data not shown). To estimate the size of IO-sensitive Ca^{2+} pool, we calculated the area under the IO-induced Ca^{2+} signals. On average, the area under the IO-induced Ca^{2+} curve was equal to 52 ± 11 μM•s (n = 19) for EGFP-transfected DKO cells, 33 ± 9 μM•s (n = 21) for EGFP+PS1–transfected DKO cells, and 31 ± 14 μM•s (n = 18) for EGFP+A79V–transfected DKO cells (Figure 3B and Table 1). Transfection with other FAD mutants had no significant effect on the size of IO-sensitive Ca^{2+} pool (Figure 3B and Table 1). To determine the effect of PS1 constructs expression on ER Ca^{2+} levels, we directly measured ER Ca^{2+} concentration ($[Ca^{2+}]_{ER}$) of transfected DKO MEFs with low-affinity Ca^{2+} imaging dye Mag-Fura-2 (16). Consistent with the previous findings (10) we found that $[Ca^{2+}]_{ER}$ levels were equal to 183 ± 42 μM (n = 18) in EGFP-transfected DKO cells, 108 ± 21 μM (n = 17) in EGFP+PS1–transfected DKO cells, and 114 ± 28 μM (n = 23) in EGFP+A79V–transfected DKO cells (Figure 3C and Table 1). The $[Ca^{2+}]_{ER}$ levels in DKO cells transfected with other FAD mutants were not significantly different from the $[Ca^{2+}]_{ER}$ levels in DKO cell transfected with EGFP plasmid alone (Figure 3C and Table 1). From these results we concluded that expression of WT PS1 or A79V FAD mutant, but not L166P, A246E, E273A, G384A, and P436Q FAD mutants, restored the size of IO-sensitive Ca^{2+} pool and the $[Ca^{2+}]_{ER}$ levels in DKO cells to the levels observed in WT MEFs (Figure 3C and Table 1).

To rule out potential artifacts resulting from transient overexpression of PS1 constructs in DKO cells, we performed a series of Ca^{2+} imaging experiments with DKO MEFs stably transfected with WT PS1 (human PS1 [hPS1] line), and L166P, A246E, and G384A FAD rescue constructs. The expression of PS1 rescue con-

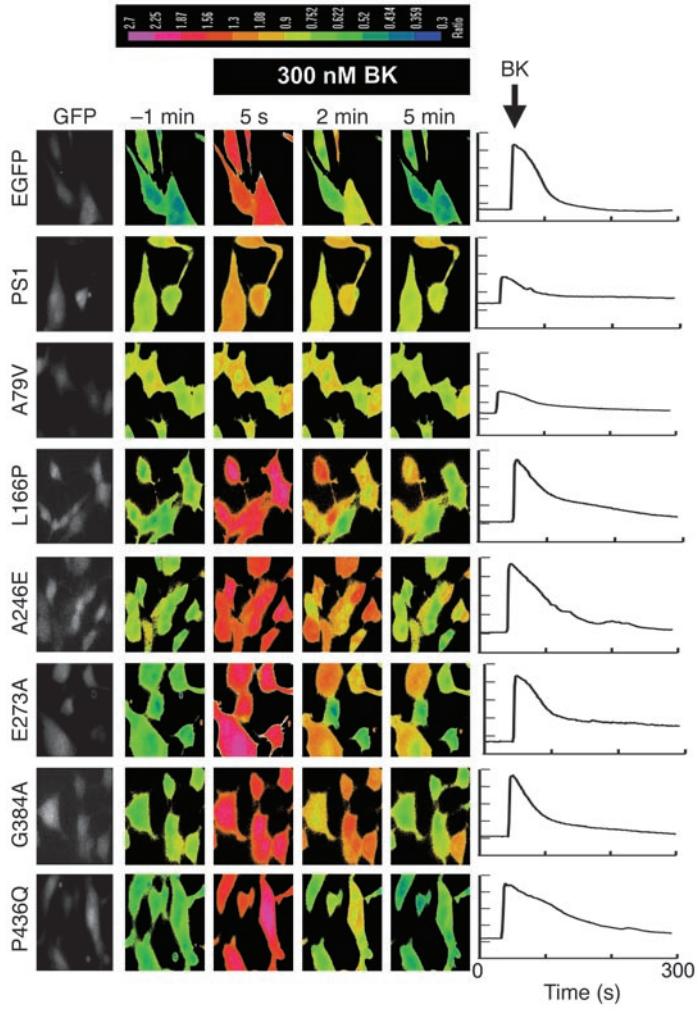

Figure 2

Rescue of Ca^{2+} signaling defects in DKO MEFs with PS1-FAD mutants. The representative images of BK-induced Ca^{2+} responses in DKO cells transfected with EGFP, EGFP+PS1, EGFP+PS1-A79V, EGFP+PS1-L166P, EGFP+PS1-A246E, EGFP+PS1-E273A, EGFP+PS1-G384A, and EGFP+PS1-P436Q expression plasmids. The 340:380 Fura-2 ratio images shown are prior to application of BK (–1 min) and 5 seconds, 2 minutes, and 5 minutes after BK application. The 340:380 Fura-2 ratios are presented using pseudocolor scale (the calibration bar is shown at top). The GFP images were used to identify transfected cells. The representative Ca^{2+} traces recorded in individual transfected DKO cells are shown at right for each expression construct.

structs in these stable lines was confirmed by Western blotting (Figure 4A). In Ca^{2+} imaging experiments with these cells we found that addition of IO induced large Ca^{2+} responses in DKO, L166P, A246E, and G384A cell lines and much smaller Ca^{2+} responses in WT MEF and hPS1 rescue cell lines (Figure 4B). By calculating an area under IO-induced Ca^{2+} curve, we determined that the content of IO-sensitive Ca^{2+} stores was significantly lower in WT and hPS1 rescue cells than in DKO, L166P, A246E, and G384A rescue cells (Figure 4C and Table 1). Direct measurements of $[Ca^{2+}]_{ER}$ levels with Mag-Fura-2 yielded values consistent with IO results (Figure 4D and Table 1). Thus, similar to transient transfection experiments (Figure 3), we found that the stable expression of WT PS1 but not L166P, A246E, and G384A FAD mutants in DKO cells restored IO-sensitive Ca^{2+} pool content and $[Ca^{2+}]_{ER}$ to WT MEF levels (Figure 4, C and D, and Table 1).

Rescue of Ca^{2+} signaling defects in presenilin DKO MEFs with FTD PS1 mutations. Human genetic studies identified 3 missense mutations in PS1 sequence (L113P, G183V, and Rins352) which are potentially associated with FTD (refs. 17–21; reviewed in ref. 2) (Figure 1A). Do these potentially FTD-associated mutations in PS1 sequence affect ER Ca^{2+} leak function? To answer this question we performed a series of rescue experiments by transiently transfecting DKO cells with the PS1-FTD expression plasmids (L113P, G183V, and Rins352) together with EGFP plasmid. In parallel control experiments DKO cells were transfected with EGFP plasmid alone. The transfected cells were identified by GFP fluorescence (Figure 5) and Ca^{2+} imaging experiments with transfected cells have been performed using Fura-2 fluorescent dye as described above. When Fura-2 images (Figure 5) were analyzed, we determined that the resting basal Ca^{2+} levels in DKO cells transfected with EGFP plasmid alone was on average 179 ± 27 nM (n = 26), while the basal Ca^{2+} levels in EGFP+PS1, EGFP+PS1-L113P, EGFP+PS1-G183V, and EGFP+PS1-Rins352 were 246 ± 38 nM (n = 31), 259 ± 56 nM (n = 27), 253 ± 34 nM (n = 39), and 234 ± 29 nM (n = 34), respectively (Figure 6A). The resting basal Ca^{2+} levels was significantly ($P < 0.05$) higher in PS1 and PS1-FTD transfected DKO cells when compared with DKO cells transfected with EGFP alone (Figure 6A).

When transfected DKO cells were challenged with 300 nM BK, large transient Ca^{2+} signals were observed in EGFP transfected cells (Figure 5). In contrast, significantly smaller Ca^{2+} signals were induced by BK in DKO cells transfected with EGFP+PS1, EGFP+PS1-L113P, EGFP+PS1-G183V, and EGFP+PS1-Rins352 combinations (Figure 5). On average, the difference between peak and basal Ca^{2+} levels ($\Delta[Ca^{2+}]$) in BK-stimulated DKO cells was equal to 689 ± 99 nM (n = 26) for EGFP-transfected cells, 261 ± 45 nM (n = 31) for EGFP+PS1–transfected cells, 288 ± 61 nM (n = 27) for EGFP+L113P–transfected cells, 237 ± 51 nM (n = 39) for EGFP+G183V–transfected cells, and 247± 37 nM (n = 34) for EGFP+Rins352–transfected cells (Figure 6A). The amplitude of BK-induced Ca^{2+} transients was significantly ($P < 0.05$) lower in PS1 and PS1-FTD–transfected DKO cells when compared with DKO cells transfected with EGFP alone (Figure 6A).

Consistent with results from BK experiments, we found that the application of 5 μM IO induced large and long-lasting elevation of cytosolic Ca^{2+} levels in DKO cells transfected with EGFP, but a smaller and shorter-lasting increase of Ca^{2+} in DKO cells transfected with WT PS1 or PS1-FTD mutants (data not shown). By integrating an area under IO-induced Ca^{2+} transients we found that the average content of IO-sensitive Ca^{2+} stores was equal to 55 ± 14 μM•s (n = 27) for EGFP-transfected DKO cells, 22 ± 7 μM•s (n = 21) for DKO cells transfected with EGFP+PS1, 25 ± 11 μM•s (n = 39) for DKO cells transfected with EGFP+L113P, 31 ± 13 μM•s (n = 31) for DKO cells transfected with EGFP+G183V, and 28 ± 11 μM•s (n = 26) for DKO cells transfected with EGFP+Rins352 (Figure 6B). The content of IO-sensitive Ca^{2+} stores was significantly smaller in PS1 and PS1-FTD–transfected DKO cells when compared with DKO cells transfected with EGFP alone ($P < 0.05$) (Figure 6B).

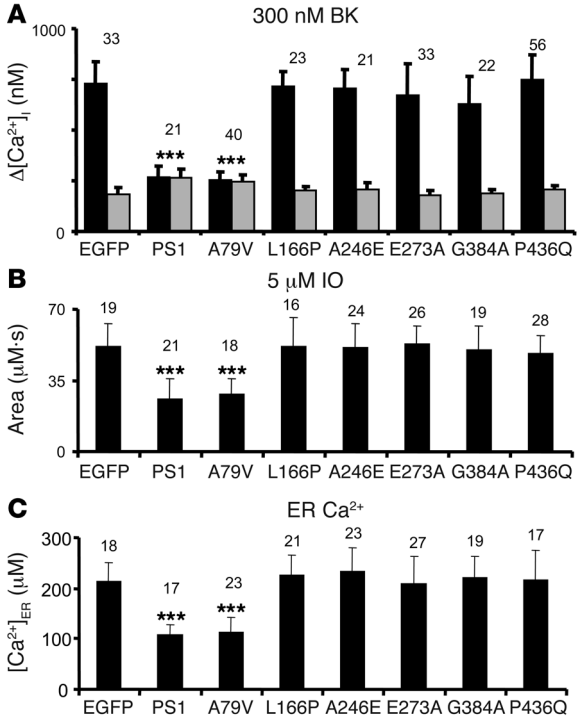

Figure 3
Summary of PS1-FAD rescue experiments. (**A**) The average basal cytosolic Ca^{2+} levels (gray bars) and the amplitude of BK-induced Ca^{2+} responses (black bars) are shown as mean ± SD for DKO cells transfected with EGFP and PS1 expression constructs (the number of cells analyzed is indicated above each set of bars). When compared with DKO cells transfected with EGFP alone, the basal Ca^{2+} levels were significantly higher and the amplitude of BK-induced Ca^{2+} responses was significantly smaller in DKO cells transfected with EGFP+PS1 and EGFP+PS1-A79V combinations. $[Ca^{2+}]_i$, intracellular Ca^{2+} concentration. (**B**) The average size of IO-releasable Ca^{2+} pool is shown as mean ± SD for DKO cells transfected with EGFP and PS1 expression constructs (the number of cells analyzed is shown above each bar). When compared with DKO cells transfected with EGFP alone, the size of IO-releasable Ca^{2+} pool was significantly smaller in DKO cells transfected with EGFP+PS1 and EGFP+PS1-A79V combinations. (**C**) The average $[Ca^{2+}]_{ER}$ level is shown as mean ± SD for DKO cells transfected with EGFP and PS1 expression constructs (the number of cells analyzed is shown above each bar). When compared with DKO cells transfected with EGFP alone, the $[Ca^{2+}]_{ER}$ levels were significantly smaller in DKO cells transfected with EGFP+PS1 and EGFP+PS1-A79V combinations. ***$P < 0.05$ by ANOVA.

Ca^{2+} signaling defects in human FAD primary fibroblasts. To establish the relevance of our results for human FAD, we obtained a sample of primary human fibroblasts (hFs) derived from a 56-year-old symptomatic patient with A246E mutation in PS1 (subject AG06840). The hFs from an unaffected 62-year-old spouse (who does not have any known FAD mutations) were also obtained to facilitate the control experiments (subject AG08701). The hF and A246E primary hFs were used in Fura-2 Ca^{2+} imaging experiments by following the same procedures as described above for MEFs. In these experiments, we determined that the mean basal Ca^{2+} level was equal to 217 ± 37 nM (n = 43) in control hFs. In A246E hFs, the mean basal Ca^{2+} level was equal to 173 ± 26 nM (n = 54), significantly lower ($P < 0.05$) than in control hFs. We further discovered that application of 300 nM BK induced larger Ca^{2+} responses in A246E hFs than in control hFs (Figure 7, A and B). On average, the amplitude of BK-induced Ca^{2+} responses was equal to 318 ± 71 μM (n = 43) in hFs and 629 ± 114 μM (n = 54) in A246E cells (Figure 7C and Table 1). The enhanced amplitude of BK-induced Ca^{2+} responses in A246E hFs is in agreement with the earlier observations made with hFs harboring the same mutation (9, 22). Similar to results from experiments with BK, application of 5 μM IO induced larger Ca^{2+} transients in A246E cells than in control hFs in our experiments (Figure 7D). As described above for MEFs, we calculated an area under the IO-induced Ca^{2+} curve to quantify the content of IO-sensitive Ca^{2+} stores in these cells. We found that the average content of IO-sensitive Ca^{2+} stores was equal to 19 ± 7 μM•s (n = 56) for hFs and 37 ± 12 μM•s (n = 63) for A246E cells (Figure 7E and Table 1). Direct measurements of $[Ca^{2+}]_{ER}$ with Mag-Fura-2 yielded 84 ± 19 μM Ca^{2+} (n = 34) in hFs and 169 ± 27 μM Ca^{2+} (n = 41) in hF-A246E (Figure 7, F and G, and Table 1). From these experiments, we concluded that the intracellular Ca^{2+} stores were overfilled in primary fibroblasts from the A246E patient when compared with hFs from the unaffected family member. The Ca^{2+} signaling defects observed in A246E primary hFs in our experiments are consistent with the previous studies of Ca^{2+} signaling in FAD fibroblasts (refs. 9, 22–24; but also see ref. 25).

Discussion

Mutations in PS1 and PS2 account for majority of all known FAD cases for which genetic cause has been identified (1). Many FAD mutations in presenilins result in deranged Ca^{2+} signaling, but the mechanistic explanation for these finding has been controversial (reviewed in ref. 8). Our recent discovery that presenilins function as ER Ca^{2+} leak channels (10) provided a direct link between presenilins and Ca^{2+} signaling. The results presented here and in ref. 10 indicate that most FAD mutations in presenilins have a dramatic effect on the ability of presenilins to function as ER Ca^{2+} leak channels. In experiments from this study and ref. 10, we tested 8 FAD mutations in PS1 and 1 FAD mutation in PS2 (Figure 1A and Table 1). From the 9 FAD mutations tested, 7 mutations (M146V, L166P, A246E, E273A, G384A, and P436Q mutations in PS1 and the N141I/L mutation in PS2) abolished ER Ca^{2+} leak function of presenilins. This conclusion was based on the lack of channel activity in BLM experiments with the FAD mutants and the failure of these mutants to rescue Ca^{2+} signaling defects in presenilin DKO cells (Table 1). One FAD mutation (PS1-ΔE9) appeared to be a gain-of-function mutation that enhanced Ca^{2+} channel activity of presenilins in BLM experiments (10) (Table 1). Interestingly, ER Ca^{2+} leak function was not affected by D257A mutation, which abolishes γ-secretase function of PS1 (10) (Table 1). As discussed in our previous publication (10), ER Ca^{2+} leak function of presenilins appears to be independent of their γ-secretase function.

A single mutation from 9 FAD mutations tested (PS1-A79V) had no apparent effect on ER Ca^{2+} leak function in our experiments (Table 1). Interestingly, PS1-A79V mutation resulted in a

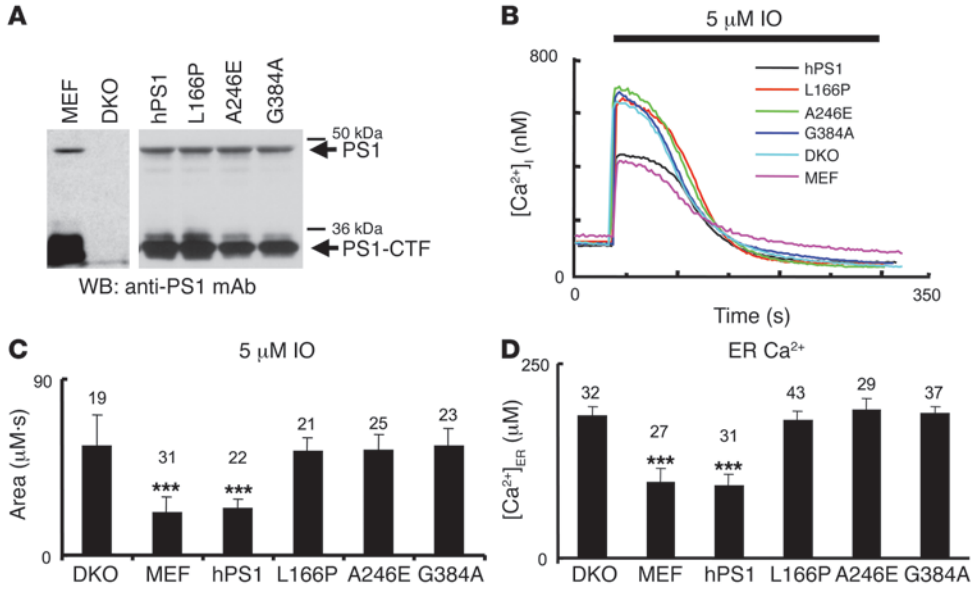

Figure 4

Ca^{2+} signals in stable DKO rescue lines. (**A**) The lysates from WT MEFs, DKO cells, and stable DKO rescue lines hPS1, PS1-L166P, PS1-A246E, and PS1-G384A were prepared and analyzed by Western blotting with anti-PS1 monoclonal antibodies. The positions of PS1 holoprotein and PS1-CTF fragment are indicated. Longer exposure was used for MEF and DKO samples than for stable rescue lines. (**B**) The representative IO-induced Ca^{2+} responses are shown for WT MEFs, DKO cells, and stable DKO rescue lines. (**C**) The average size of IO-sensitive Ca^{2+} pool is shown as mean ± SD for WT MEFs, DKO cells, and stable DKO rescue lines (the number of cells analyzed is shown above each bar). When compared with DKO cells, the size of IO-sensitive Ca^{2+} pool was significantly smaller in WT MEFs and hPS1 cells but not significantly different in FAD stable rescue lines. (**D**) The average $[Ca^{2+}]_{ER}$ in WT MEFs, DKO cells, and stable DKO rescue lines is shown as mean ± SD (the number of cells analyzed is shown above each bar). When compared with DKO cells, the $[Ca^{2+}]_{ER}$ was significantly smaller in WT MEFs and hPS1 cells but not significantly different in FAD stable rescue lines. ***$P < 0.05$ by ANOVA.

highly variable age of FAD onset and incomplete penetrance in one of the carrier families (26). FAD mutations typically have complete penetrance, and a few incompletely penetrant FAD-linked mutations such as PS1-E318G and PS1-T354I appear to represent rare polymorphisms and are not pathogenic (27–30). It remains to be determined whether the PS1-A79V mutation is pathogenic or another example of a rare polymorphism. Our results suggest that, if it is pathogenic, abnormal Ca^{2+} signaling would not be involved in the pathology resulting from this mutation. It is also possible that PS1-A79V is a mutation that results in *partial* loss of ER Ca^{2+} leak function mutation and therefore cannot be detected in our bilayer and DKO rescue experiments, which are geared toward detecting phenotypes with *complete* loss of ER Ca^{2+} leak function. The incomplete penetrance of PS1-A79V mutation discussed above may also be consistent with a partial-loss-of-function phenotype. More precise and sensitive experiments will be required to formally address this possibility.

With the exception of PS1-A79V and PS1-ΔE9, all 7 other FAD-linked mutations tested in our experiments resulted in complete loss of ER Ca^{2+} leak function of presenilins (Table 1). These results are in sharp contrast to the results obtained with 3 known FTD-associated mutations in PS1, none of which appear to affect ER Ca^{2+} leak function of PS1. Expression of FTD-associated L113P, G183V, and Rins352 PS1 mutants rescued Ca^{2+} signals in DKO cells similar to expression of WT PS1 (Figures 5 and 6). These results suggest either that these mutations are not pathogenic or that defects in ER Ca^{2+} leak pathway are not involved in FTD pathogenesis. In contrast to our findings, the insR352 mutation in PS1 has been reported to be a loss-of-function mutation for the γ-secretase activity (17). However, a recent study indicated that the insR352 mutation in PS1 is in fact not pathogenic and that FTD in the affected family results from a mutation in the progranulin gene (31). Further studies are needed to determine the pathogenic status of L113P (20) and G183V (19) FTD-associated mutations in PS1. Additional investigation is also necessary to analyze functional effects of 2 more recently described FTD-associated PS1 mutations, L226F and L424H (32).

Some of the FAD mutants analyzed here and in ref. 10 (PS1-M146V/L, PS2-N141I/L, PS1-ΔE9, PS1-A246Q/E) were previously linked to abnormal Ca^{2+} signaling (8). Our new results indicate that L166P, E273A, G384A, and P436Q FAD mutants in PS1 are also linked to abnormal Ca^{2+} signaling due to impaired ER Ca^{2+} leak function (Table 1). The impaired ER Ca^{2+} leak function of PS1 FAD mutants observed here and in ref. 10 is consistent with the increased inositol 1,4,5-triphosphate–induced Ca^{2+} release in *Xenopus* oocytes expressing PS1-M146V and PS2-N141I FAD mutants (33–35), in synaptosomes and cortical neurons from the PS1-M146V mutant knockin mouse (36, 37), in hippocampal neurons from PS2-N141I and PS1-A246E transgenic mice (38), and in hFs from PS1-A246E patients (9, 22). However, our results differ from the data obtained in studies of PS1-M146L, PS1-A246E, and PS2-N141I FAD mutants recently reported by Zatti et al. (25). In contrast to our findings, these authors found that expression of these FAD mutants causes either no effect or reduction of ER Ca^{2+} content and decreased inositol 1,4,5-triphosphate receptor–mediated Ca^{2+} release. The exact nature of this discrepancy is unclear at the moment and will require further investigation.

The mutations analyzed in the present paper and in the previous study are spread across the sequence of presenilins (Figure 1A) and correspond to FAD cases with varying ages of onset (Table 1). We could not detect from these results any particular "hot-spot" region or pattern that could be used to predict which mutations influenced ER Ca^{2+} leak function of presenilins and which did not. With 156 FAD mutations identified in the sequence of PS1 and 10 FAD mutations in the sequence PS2 (1, 39), future experimentation will be required to identify all FAD mutations in presenilins that affect their ER Ca^{2+} leak function. However, from the results obtained so far (Table 1), we can conclude

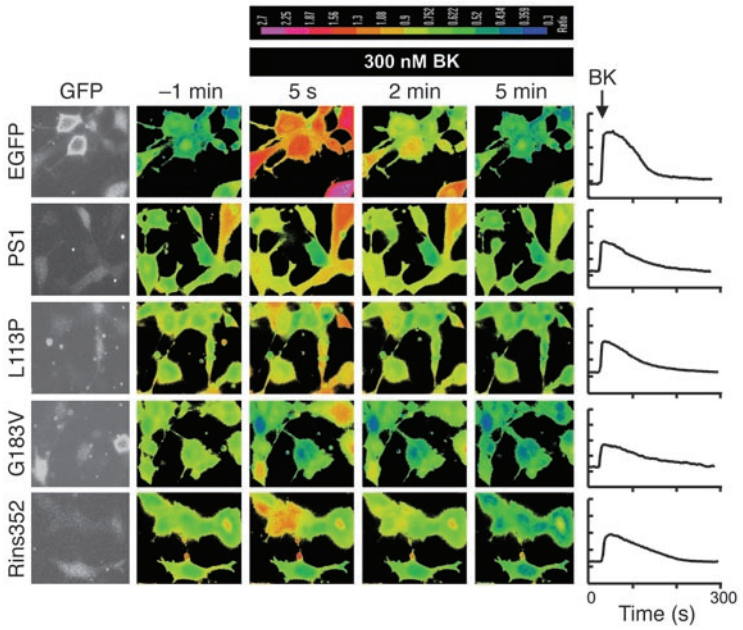

Figure 5
Rescue of Ca^{2+} signaling defects in DKO MEFs with PS1-FTD mutants. The representative images of BK-induced Ca^{2+} responses in DKO cells transfected with EGFP, EGFP+PS1, EGFP+PS1-L113P, EGFP+PS1-G183V, and EGFP+PS1-Rins352 expression plasmids. The 340:380 Fura-2 ratio images are shown prior to application of BK (–1 min) and 5 seconds, 2 minutes, and 5 minutes after BK application. The 340:380 Fura-2 ratios are presented using a pseudocolor scale (the calibration bar is shown at top). The GFP images were used to identify transfected cells. The representative Ca^{2+} traces recorded in individual transfected DKO cells are shown for each expression construct on the right.

that many FAD point mutations in presenilins result in loss of ER Ca^{2+} leak function. As discussed previously (10), the autosomal-dominant character of these mutations may be explained by a dominant-negative effect of mutant presenilin allele on Ca^{2+} channel function of WT alleles. Our results are in general agreement with the hypotheses that FAD is associated with a loss of presenilin function (40–42) and that disturbed Ca^{2+} homeostasis contributes to AD pathogenesis (8, 11–13). Additional studies will be required to investigate the connection between defective Ca^{2+} signaling and neurodegeneration in AD.

Methods

Expression constructs and recombinant baculoviruses. The WT PS1 expression construct and generation of PS1 baculovirus has been previously described (10). The PS1-G384A and PS1-A246E constructs were kindly provided by Christine Van Broeckhoven (University of Antwerp, Antwerp, Belgium) (43) and the PS1-L166P construct was kindly provided by Christian Haass (University of Munich, Munich, Germany) (44). The A79V, E273A, G384A, P436Q, L113P, G183V, and Rins352 mutations in WT PS1 sequence were generated by QuikChange Site-Directed Mutagenesis Kit (Stratagene) and verified by sequencing. The PS1-FAD constructs were cloned into pFastBac1 baculovirus vector (Invitrogen) and recombinant PS1-FAD baculoviruses were generated using Bac-to-Bac System (Invitrogen) as previously described for the WT PS1 (10). The high-titer baculoviral stocks were obtained by amplification of generated viruses in Sf9 cells. For expression in DKO cells, all FAD and FTD PS1 constructs were cloned into pcDNA3 or pmSCV mammalian expression vectors.

BLM reconstitution experiments. WT and mutant presenilins were expressed in Sf9 cells as previously described (10). The ER microsomes were isolated from Sf9 cell homogenates by differential centrifugation as previously described (45) and stored at –80°C. The expression of PS1 in Sf9 cells was confirmed by Western blotting of isolated microsomal preparations with monoclonal anti-PS1 antibodies (catalog no. MAB5232; Chemicon

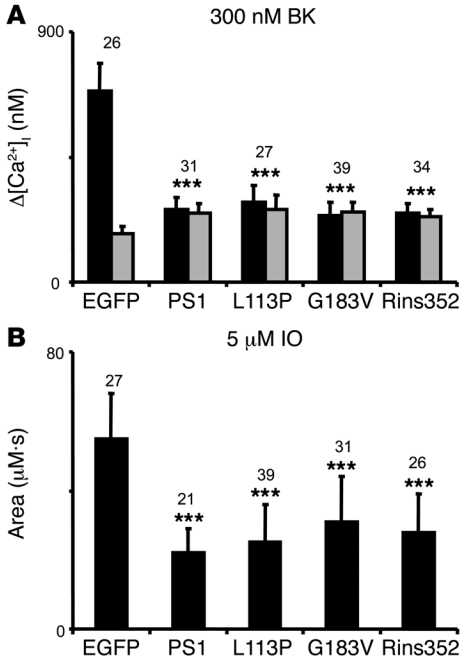

Figure 6
Summary of PS1-FTD rescue experiments. (**A**) The average basal cytosolic Ca^{2+} levels (gray bars) and the amplitude of BK-induced Ca^{2+} responses (black bars) are shown as mean ± SD for DKO cells transfected with EGFP and PS1 expression constructs (the number of cells analyzed is shown above each set of bars). When compared with DKO cells transfected with EGFP alone, the basal Ca^{2+} levels were significantly higher and the amplitude of BK-induced Ca^{2+} response was significantly smaller in DKO cells transfected with EGFP+PS1, EGFP+PS1-L113P, EGFP+PS1-G183V, and EGFP+PS1-Rins352. (**B**) The average size of IO-releasable Ca^{2+} pool is shown as mean ± SD for DKO cells transfected with EGFP and PS1 expression constructs (the number of cells analyzed is shown above each bar). When compared with DKO cells transfected with EGFP alone, the size of IO-releasable Ca^{2+} pool was significantly smaller in DKO cells transfected with EGFP+PS1, EGFP+PS1-L113P, EGFP+PS1-G183V, and EGFP+PS1-Rins352 combinations. ***$P < 0.05$ by ANOVA.

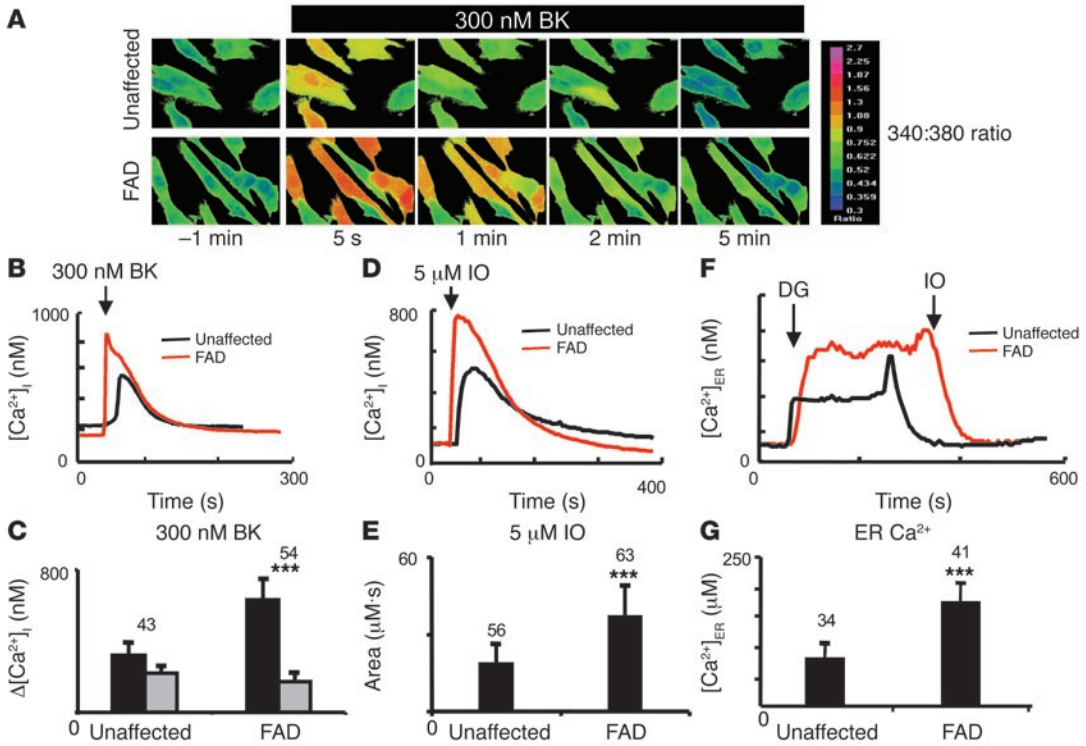

Figure 7

Ca^{2+} signals in human primary fibroblasts from the FAD patient. (**A**) The representative Fura-2 images of BK-induced Ca^{2+} responses are shown for hFs from symptomatic PS1-A246E FAD patient and for hFs from the unaffected spouse. The Fura-2 340:380 ratios are presented as explained in the Figure 2 legend. (**B**) The time course of BK-induced Ca^{2+} signals in representative experiments with hFs and hF-A246E cells. (**C**) The average basal cytosolic Ca^{2+} levels (gray bars) and the amplitude of BK-induced Ca^{2+} responses (black bars) are shown as mean ± SD for hFs and hF-A246E cells (the number of cells analyzed is shown above each set of bars). When compared with hFs, the basal Ca^{2+} levels were significantly lower and the amplitude of BK-induced Ca^{2+} response was significantly larger in hF-A246E cells. (**D**) The time course of IO-induced Ca^{2+} signals in representative experiments with hFs and hF-A246E cells. (**E**) The average size of IO-sensitive Ca^{2+} pool is shown as mean ± SD for hFs and hF-A246E cells (the number of cells analyzed is shown above each bar). When compared with hFs, the size of IO-sensitive Ca^{2+} pool was significantly larger in hF-A246E cells. (**F**) Representative ER Ca^{2+} traces recorded by ER-loaded Mag-Fura-2 in hFs and hF-A246E cells. The cells were loaded with Mag-fura-2 and permeabilized by 10 μM digitonin (DG) in a buffer containing 170 nM Ca^{2+} and 3 mM ATP. The ER membrane was permeabilized with 5 μM IO in Ca^{2+}-free buffer at the end of the experiment. The Mag-Fura-2 340:380 ratios were converted to $[Ca^{2+}]_{ER}$ as described in Methods. (**G**) The average $[Ca^{2+}]_{ER}$ determined for hFs and hF-A246E cells are shown as mean ± SD (the number of cells analyzed is shown above each bar). When compared with control hFs, the ER Ca^{2+} concentration was significantly higher in hF-A246E cells. ***$P < 0.05$ by ANOVA.

International). As a loading control, the samples were blotted with monoclonal antibodies against β-actin (catalog no. MAB1501; Chemicon International). The samples used for Western blotting were maintained at 37°C prior to loading on the gel. The isolated ER microsomes were fused with BLMs, and recordings of presenilin-supported currents were performed and analyzed as previously described (10). In these experiments the *trans* (intraluminal) side of the BLM contained 50 mM Ba^{2+}/HEPES (pH 7.35) and the *cis* (cytosolic) side contained 100 mM Tris/HEPES (pH 7.35). The *cis* chamber was held at virtual ground and the *trans* chamber was voltage clamped (BC-525C bilayer clamp; Warner Instruments) to 0 mV, +10 mV, and –10 mV as indicated (Figure 1C). The current across the BLM was amplified (OC-725C), filtered at 5 kHz, digitized (Digidata 1200; Axon Instruments), and stored on a computer hard drive and recordable optical discs. For presentation, the current traces were digitally filtered at 200 Hz (pClamp 6.0; Axon Instruments). For off-line computer analysis, stationary noise analysis method was used as previously described (10). Using WinEDR version 2.4.3 software (BioLogic) (46), the currents were filtered at 100 Hz and the mean current (I) and the current variance (δ^2) was determined for the currents measured before addition of ER microsomes (I_{BLM} and δ_{BLM}^2) and after fusion of ER microsomes (I_{PS} and δ_{PS}^2) in the same experiment. The unitary size of PS1-mediated currents (i_{PS}) was then estimated for each experiment from the noise analysis equation: $i_{PS} = (\delta_{PS}^2 - \delta_{BLM}^2)/(I_{PS} - I_{BLM})$ as previously described (10).

Ca^{2+} imaging experiments. The presenilin-DKO MEFs and the hPS1, L166P, A246E, G384A stable rescue lines have been previously described (15, 44). Primary hFs from a 56-year-old symptomatic FAD patient with PS1-A246E mutation (subject AG06840) and the control hFs from the 62-year-old unaffected spouse (subject AG08701) were obtained from the Coriell Cell Repositories (Coriell Institute for Medical Research). Ca^{2+} imaging experiments with MEFs and hFs were performed as previously described (10). Briefly, the cells were cultured on poly-D-lysine–coated (Sigma-Aldrich) 12-mm round glass coverslips and loaded with 5 μM Fura-2, AM (Invitrogen) in HCSS buffer (120 mM NaCl, 5.4 mM KCl, 0.8 mM $MgCl_2$, 2 mM $CaCl_2$, 15 mM glucose, and 20 mM HEPES, pH 7.3) for 45 minutes at 37°C. For Ca^{2+} imaging experiments the coverslips were mounted onto a recording/perfusion chamber (RC-26G; Warner Instruments), positioned on a movable stage of an Olympus IX-70 inverted microscope, and washed with Ca^{2+}-deficient HCSS buffer (buffered with EGTA to 50 nM Ca^{2+}). In

Ca^{2+} imaging experiments, the cells were intermittently excited by 340-nM and 380-nM UV light using DeltaRam illuminator (Photon Technology International) using a Fura-2 dichromic filter cube (Chroma Technology) and ×60 UV-grade oil-immersed objective (Olympus). The emitted light was collected by an IC-300 camera (Photon Technology International), and the images were digitized by the ImageMaster Pro software (version 1.49; Photon Technology International). Baseline (6-minute) measurements were obtained prior to bath application of drugs. The drugs — 300 nM BK and 5 μM IO (both from Sigma-Aldrich) — were dissolved in Ca^{2+}-deficient HCSS buffer prior to application to the cells. Images at 340-nm and 380-nm excitation wavelengths were captured every 2 seconds and shown as 340:380 image ratios at the time points indicated (Figure 2, Figure 5, and Figure 7A). Background fluorescence was determined according to the manufacturer's recommendations (Photon Technology International) and subtracted. The absolute values of free cytosolic Ca^{2+} concentrations ($[Ca^{2+}]$) in these experiments were determined from the equation (47).

$[Ca^{2+}]_i = K_d (R - R_{min})/(R_{max} - R) S_{f'380}/S_{b'380}$, where K_d is the affinity of Fura-2 for Ca^{2+} (140 nM), R is the experimentally determined 340:380 ratio, R_{max} is the 340:380 ratio for Fura-2 saturated with Ca^{2+} (determined by application of 20 mM Ca^{2+} and 10 μM IO at the end of the experiment), R_{min} is the 340:380 ratio for Ca^{2+}-free Fura-2 (determined by addition of 10 mM EGTA following R_{max} determination), and $S_{f'380}/S_{b'380}$ is the ratio of fluorescence intensity of Ca^{2+}-free and Ca^{2+}-bound form of Fura-2 at 380 nM ($S_{f'380}/S_{b'380} = 2$ in our experiments).

In transient transfection rescue experiments, DKO cells were transfected using Lipofectamine (Invitrogen) by pEGFP-C3 plasmid (Clontech) or by a 1:3 mixture of pEGFP-C3 and PS1 expression plasmids. The Ca^{2+} imaging experiments were performed and analyzed as described above 48 hours after transfection. The transfected cells were identified by GFP imaging using GFP filter cube (Chroma) prior to Fura-2 Ca^{2+} imaging as previously described (10).

ER Ca^{2+} measurements. The ER Ca^{2+} levels in MEFs were measured using Mag-Fura-2 as previously described (10, 16), with the Photon Technology International Ca^{2+} imaging setup described above. Briefly, the cells were first loaded with 2 μM Mag-Fura-2, AM (Invitrogen) in HCSS buffer for 30 minutes at 37°C and permeabilized by application of 10 μM digitonin in the intracellular buffer (125 mM KCl, 25 mM NaCl, 10 mM HEPES, 0.1 mM $MgCl_2$; pH 7.3) containing 170 nM free Ca^{2+} (clamped by 5 mM EGTA) and 3 mM ATP. Mag-Fura-2 signals were collected as 340:380 ratios for the duration of the experiment, then the ER membrane was permeabilized with 5 μM IO and the cells were washed with an ATP- and Ca^{2+}-free calibration buffer (125 mM KCl, 25 mM NaCl, 10 mM HEPES, pH 7.3) containing 0.8 mM EGTA. The Mag-Fura-2 signals were calibrated in the presence of 10 μM IO using a series of calibration buffers with free Ca^{2+} clamped to defined concentrations by 1 mM nitrilotriacetic acid as previously described (10). Based on these calibration results, the 340:380 Mag-Fura-2 ratios were converted to $[Ca^{2+}]_{ER}$ concentrations using the following empirical formula: $[Ca^{2+}]_{ER} = 141 (R - 0.49) / (1.42 - R)$, where $[Ca^{2+}]_{ER}$ is intraluminal ER Ca^{2+} concentration in μM and R is the 340:380 ratio reported by Mag-Fura-2 in our experiments.

Acknowledgments

We thank Gang Yu for helpful discussions and Janet Young for administrative assistance. We are thankful to Christine Van Broeckhoven for providing the PS1-G384A and PS1-A246E constructs, Christian Haass for providing the PS1-L166P construct, and Coriell Cell Repositories for providing PS1-A246E and control human fibroblast samples. I. Bezprozvanny is a holder of the Carla Cocke Francis Professorship in Alzheimer's Research and is supported by the Welch Foundation, National Institute of Neurological Disorders and Stroke grant R01 NS38082, and the Alzheimer's Association Research Grant IIRG-06-24703. B. de Strooper is supported by a Pioneer Award from the Alzheimer's Association, the Katholieke Universiteit Leuven (grant GOA 2004/12), and the Federal Office for Scientific Affairs, Belgium (grant IUAP P5/19).

Received for publication September 24, 2006, and accepted in revised form February 13, 2007.

Address correspondence to: Ilya Bezprozvanny, Department of Physiology, ND12.502, University of Texas Southwestern Medical Center at Dallas, Dallas, Texas 75390-9040, USA. Phone: (214) 645-6017; Fax: (214) 645-6018; E-mail: Ilya.Bezprozvanny@UTSouthwestern.edu.

1. Tandon, A., and Fraser, P. 2002. The presenilins. *Genome Biol.* **3**:reviews3014.
2. Hutton, M. 2004. Presenilin mutations associated with fronto-temporal dementia. *Ann. Neurol.* **55**:604–606.
3. Laudon, H., et al. 2005. A nine-transmembrane domain topology for presenilin 1. *J. Biol. Chem.* **280**:35352–35360.
4. Spasic, D., et al. 2006. Presenilin-1 maintains a nine-transmembrane topology throughout the secretory pathway. *J. Biol. Chem.* **281**:26569–26577.
5. Annaert, W.G., et al. 1999. Presenilin 1 controls gamma-secretase processing of amyloid precursor protein in pre-golgi compartments of hippocampal neurons. *J. Cell Biol.* **147**:277–294.
6. De Strooper, B., et al. 1998. Deficiency of presenilin-1 inhibits the normal cleavage of amyloid precursor protein. *Nature.* **391**:387–390.
7. Wolfe, M.S., et al. 1999. Two transmembrane aspartates in presenilin-1 required for presenilin endoproteolysis and gamma-secretase activity. *Nature.* **398**:513–517.
8. Smith, I.F., Green, K.N., and LaFerla, F.M. 2005. Calcium dysregulation in Alzheimer's disease: recent advances gained from genetically modified animals. *Cell Calcium.* **38**:427–437.
9. Ito, E., et al. 1994. Internal Ca2+ mobilization is altered in fibroblasts from patients with Alzheimer disease. *Proc. Natl. Acad. Sci. U. S. A.* **91**:534–538.
10. Tu, H., et al. 2006. Presenilins form ER calcium leak channels, a function disrupted by mutations linked to familial Alzheimer's disease. *Cell.* **126**:981–993.
11. Khachaturian, Z.S. 1989. Calcium, membranes, aging, and Alzheimer's disease. Introduction and overview. *Ann. N. Y. Acad. Sci.* **568**:1–4.
12. Mattson, M.P., et al. 2000. Calcium signaling in the ER: its role in neuronal plasticity and neurodegenerative disorders. *Trends Neurosci.* **23**:222–229.
13. LaFerla, F.M. 2002. Calcium dyshomeostasis and intracellular signalling in Alzheimer's disease. *Nat. Rev. Neurosci.* **3**:862–872.
14. Hofer, A.M., Curci, S., Machen, T.E., and Schulz, I. 1996. ATP regulates calcium leak from agonist-sensitive internal calcium stores. *FASEB J.* **10**:302–308.
15. Herreman, A., et al. 2000. Total inactivation of gamma-secretase activity in presenilin-deficient embryonic stem cells. *Nat. Cell Biol.* **2**:461–462.
16. Hofer, A.M. 1999. Measurement of free [Ca2+] changes in agonist-sensitive internal stores using compartmentalized fluorescent indicators. *Methods Mol. Biol.* **114**:249–265.
17. Amtul, Z., et al. 2002. A presenilin 1 mutation associated with familial frontotemporal dementia inhibits gamma-secretase cleavage of APP and notch. *Neurobiol. Dis.* **9**:269–273.
18. Rogaeva, E.A., et al. 2001. Screening for PS1 mutations in a referral-based series of AD cases: 21 novel mutations. *Neurology.* **57**:621–625.
19. Dermaut, B., et al. 2004. A novel presenilin 1 mutation associated with Pick's disease but not beta-amyloid plaques. *Ann. Neurol.* **55**:617–626.
20. Raux, G., et al. 2000. Dementia with prominent frontotemporal features associated with L113P presenilin 1 mutation. *Neurology.* **55**:1577–1578.
21. Tang-Wai, D., et al. 2002. Familial frontotemporal dementia associated with a novel presenilin-1 mutation. *Dement. Geriatr. Cogn. Disord.* **14**:13–21.
22. Etcheberrigaray, R., et al. 1998. Calcium responses in fibroblasts from asymptomatic members of Alzheimer's disease families. *Neurobiol. Dis.* **5**:37–45.
23. Peterson, C., Ratan, R.R., Shelanski, M.L., and Goldman, J.E. 1986. Cytosolic free calcium and cell spreading decrease in fibroblasts from aged and Alzheimer donors. *Proc. Natl. Acad. Sci. U. S. A.* **83**:7999–8001.
24. Hirashima, N., et al. 1996. Calcium responses in human fibroblasts: a diagnostic molecular profile for Alzheimer's disease. *Neurobiol. Aging.* **17**:549–555.
25. Zatti, G., et al. 2006. Presenilin mutations linked to familial Alzheimer's disease reduce endoplasmic reticulum and Golgi apparatus calcium levels. *Cell Calcium.* **39**:539–550.
26. Cruts, M., et al. 1998. Estimation of the genetic contribution of presenilin-1 and -2 mutations in a population-based study of presenile Alzheimer

disease. *Hum. Mol. Genet.* **7**:43–51.
27. Lee, P., Medina, L., and Ringman, J.M. 2006. The Thr354Ile substitution in PSEN1: disease-causing mutation or polymorphism? *Neurology.* **66**:1955–1956.
28. Dermaut, B., et al. 1999. The Glu318Gly substitution in presenilin 1 is not causally related to Alzheimer disease. *Am. J. Hum. Genet.* **64**:290–292.
29. Goldman, J.S., et al. 2005. Presenilin 1 Glu318Gly polymorphism: interpret with caution. *Arch. Neurol.* **62**:1624–1627.
30. Mattila, K.M., et al. 1998. The Glu318Gly mutation of the presenilin-1 gene does not necessarily cause Alzheimer's disease. *Ann. Neurol.* **44**:965–967.
31. Boeve, B.F., et al. 2006. Frontotemporal dementia and parkinsonism associated with the IVS1+1G->A mutation in progranulin: a clinicopathologic study. *Brain.* **129**:3103–3114.
32. Zekanowski, C., et al. 2006. Two novel presenilin 1 gene mutations connected with frontotemporal dementia-like clinical phenotype: genetic and bioinformatic assessment. *Exp. Neurol.* **200**:82–88.
33. Leissring, M.A., Paul, B.A., Parker, I., Cotman, C.W., and LaFerla, F.M. 1999. Alzheimer's presenilin-1 mutation potentiates inositol 1,4,5-trisphosphate-mediated calcium signaling in Xenopus oocytes. *J. Neurochem.* **72**:1061–1068.
34. Leissring, M.A., Parker, I., and LaFerla, F.M. 1999. Presenilin-2 mutations modulate amplitude and kinetics of inositol 1, 4,5-trisphosphate-mediated calcium signals. *J. Biol. Chem.* **274**:32535–32538.
35. Leissring, M.A., LaFerla, F.M., Callamaras, N., and Parker, I. 2001. Subcellular mechanisms of presenilin-mediated enhancement of calcium signaling. *Neurobiol. Dis.* **8**:469–478.
36. Begley, J.G., Duan, W., Chan, S., Duff, K., and Mattson, M.P. 1999. Altered calcium homeostasis and mitochondrial dysfunction in cortical synaptic compartments of presenilin-1 mutant mice. *J. Neurochem.* **72**:1030–1039.
37. Stutzmann, G.E., Caccamo, A., LaFerla, F.M., and Parker, I. 2004. Dysregulated IP3 signaling in cortical neurons of knock-in mice expressing an Alzheimer's-linked mutation in presenilin1 results in exaggerated Ca2+ signals and altered membrane excitability. *J. Neurosci.* **24**:508–513.
38. Schneider, I., et al. 2001. Mutant presenilins disturb neuronal calcium homeostasis in the brain of transgenic mice, decreasing the threshold for excitotoxicity and facilitating long-term potentiation. *J. Biol. Chem.* **276**:11539–11544.
39. Larner, A.J., and Doran, M. 2006. Clinical phenotypic heterogeneity of Alzheimer's disease associated with mutations of the presenilin-1 gene. *J. Neurol.* **253**:139–158.
40. Saura, C.A., et al. 2004. Loss of presenilin function causes impairments of memory and synaptic plasticity followed by age-dependent neurodegeneration. *Neuron.* **42**:23–36.
41. Shen, J., and Kelleher, R.J., 3rd. 2007. The presenilin hypothesis of Alzheimer's disease: evidence for a loss-of-function pathogenic mechanism. *Proc. Natl. Acad. Sci. U. S. A.* **104**:403–409.
42. De Strooper, B. 2007. Loss-of-function presenilin mutations in Alzheimer disease. *EMBO Rep.* **8**:1–6.
43. De Jonghe, C., et al. 1999. Evidence that Abeta42 plasma levels in presenilin-1 mutation carriers do not allow for prediction of their clinical phenotype. *Neurobiol. Dis.* **6**:280–287.
44. Bentahir, M., et al. 2006. Presenilin clinical mutations can affect gamma-secretase activity by different mechanisms. *J. Neurochem.* **96**:732–742.
45. Tu, H., et al. 2002. Functional characterization of the type 1 inositol 1,4,5-trisphosphate receptor coupling domain SII$^{(+/-)}$ splice variants and the *opisthotonos* mutant form. *Biophys. J.* **82**:1995–2004.
46. Dempster, J. 2001. *The laboratory computer: a practical guide for neuroscientists and physiologists.* Academic Press. London, United Kingdom. 354 pp.
47. Grynkiewicz, G., Poenie, M., and Tsien, R.Y. 1985. A new generation of Ca2+ indicators with greatly improved fluorescence properties. *J. Biol. Chem.* **260**:3440–3450.
48. Mattson, M.P., Guo, Q., Furukawa, K., and Pedersen, W.A. 1998. Presenilins, the endoplasmic reticulum, and neuronal apoptosis in Alzheimer's disease. *J. Neurochem.* **70**:1–14.